and D. M. Noden, *Am. J. Anat.* **166**, 445 (1983); G. Serbedzija, M. Bronner-Fraser, S. F. Fraser, *Development* **106**, 806 (1989).
8. N. Le Douarin, *Dev. Biol.* **30**, 217 (1973); C. Le Lievre and N. Le Douarin, *J. Embryol. Exp. Morphol.* **34**, 125 (1975).
9. G. C. Tucker, H. Aoyama, M. Lipinski, T. Tursz, J. P. Thiery, *Cell Differ.* **14**, 223 (1984).
10. M. Vincent and J. P. Thiery, *Dev. Biol.* **103**, 468 (1984).
11. J. Sechrist, G. N. Serbedzija, T. Scherson, S. E. Fraser, M. Bronner-Fraser, *Development* **118**, 691 (1993).
12. G. Zon and W. J. Stec, in *Oligonucleotides and Analogues*, F. Eckstein, Ed. (Oxford Univ. Press, Oxford, 1991), pp. 87–108.
13. The random oligo mixture was synthesized to have an overall nucleotide composition similar to the average base composition of oligos A and B (Fig. 1) and of an antisense oligo to chick *snail*, according to the following program: A/G G A/G C/T T C/T G A/G A/G C/T C/T C A/G A/G A. The control embryos were treated with this oligo mixture at a concentration of 80 μM. Anti-*Slug* oligos A and B were used at 12 μM.
14. D. A. T. New, *J. Embryol. Exp. Morphol.* **3**, 326 (1955).
15. Blastoderms of the required ages (20 to 30 hours of egg incubation) were explanted as for culture by the technique of New (*14*), in which they rest inverted (endoderm side up), attached as they normally are by their periphery to the vitelline membrane, which is stretched over a ring. The membrane separates the embryo from an underlying pool of growth medium composed of egg albumen (90%) and Pannett and Compton chick saline (10%). For oligo treatment, the blastoderms were detached from their membranes and incubated, ectoderm side up, in 1 ml of a protein-free medium in 35-mm plastic dishes, six to eight per dish. This medium was composed of Hanks balanced salt solution (80%) and Liebovitz TCM (20%) with Ca and Mg^{2+}, each at a concentration of 0.2 mM. Oligos were added from stock concentrates frozen as aliquots in diethyl pyrocarbonate–treated water to give the working concentrations [see text and (*13*)] before incubation for 2 hours at 38°C in humidified air. Blastoderms were then replaced in an inverted position on the original membranes and repositioned while the saline was drained from within the culture ring. The blastoderms reattached and continued to spread on the membranes during the following 6 to 24 hours, until stages of 7 to 15 segmented somites were reached.
16. G. C. Schoenwolf and J. L. Smith, *Development* **109**, 243 (1990).
17. Antisense oligos to chick *snail* have specific effects on somite segmentation but leave neural tube architecture normal (J. Cooke and M. A. Nieto, unpublished observations).
18. R. Bellairs, in *Developmental and Evolutionary Aspects of the Neural Crest*, P. Maderson, Ed. (Wiley, New York, 1987), pp. 123–145.
19. Candidates for regulation by *Slug* could be genes for such molecules as cadherins [M. Takeichi, *Science* **251**, 1451 (1991)] or integrins [(R. O. Hynes, *Cell* **69**, 11 (1992)]. Functional interference studies have shown that matrix-integrin interactions are important for gastrulation [(T. Darribere, K. M. Yamada, K. E. Johnson, J. C. Boucaut, *Dev. Biol.* **126**, 182 (1988)] and for neural crest migration [T. Lallier and M. Bronner-Fraser, *Science* **259**, 692 (1993)], that E-cadherin is involved in the maintenance of epithelial phenotype in epiblast cells [C. A. Burdsal, C. H. Damsky, R. A. Pedersen, *Development* **118**, 829 (1993)], and that impairment of N-cadherin function produces distorted neural tubes and ectopic neural crest cells [M. Bronner-Fraser, J. J. Wolf, B. A. Murray, *Dev. Biol.* **153**, 291 (1992)].
20. K. Basler, T. Edlund, T. M. Jessell, T. Yamada, *Cell* **73**, 687 (1993).
21. Hybridizations were done on paraformaldehyde-fixed embryos by use of a modification of the method described by D. G. Wilkinson and M. A. Nieto [*Methods Enzymol.* **225**, 361 (1993)]. In particular, embryos up to stage 10 were treated with proteinase K for 5 min. Digoxigenin-labeled RNA probes corresponded to nucleotides 1 to 358 and 493 to 1922 from the *Slug* sequence.
22. We thank K. Roberts for help in sequencing *Slug* and M. Placzek and A. Furley for criticism of draft manuscripts. An EDBO short-term fellowship to M.A.N. allowed completion of this work.

22 November 1993; accepted 1 March 1994

Microtubule Dynamics Modulated by Guanosine Triphosphate Hydrolysis Activity of β-Tubulin

Ashley Davis,* Carleton R. Sage, Cynthia A. Dougherty, Kevin W. Farrell

Microtubule dynamic instability underlies many cellular functions, including spindle morphogenesis and chromosome movement. The role of guanosine triphosphate (GTP) hydrolysis in dynamic instability was investigated by introduction of four mutations into yeast β-tubulin at amino acids 103 to 109, a site thought to participate in GTP hydrolysis. Three of the mutations increased both the assembly-dependent rate of GTP hydrolysis and the average length of steady-state microtubules over time, a measure of dynamic instability. The fourth mutation did not substantially affect the rate of GTP hydrolysis or the steady-state microtubule lengths. These results demonstrate that the rate of GTP hydrolysis can modulate microtubule length and hence dynamic instability.

Microtubules are composed of tubulin, an α-β heterodimer that binds GTP exchangeably at the β subunit E site. During microtubule assembly the E-site GTP is hydrolyzed to yield a phosphate ion, which is temporarily bound to the microtubule, and guanosine diphosphate (GDP)–tubulin, which incorporates into the microtubule lattice (*1*). Microtubules are thought to be stabilized by a "cap" (*2*) of GTP-tubulin or [GDP + inorganic phosphate (P_i)]–tubulin subunits at microtubule ends, and the loss of this cap may result in rapid microtubule depolymerization. Random loss and regain of the cap can thus account for the stochastic growing and shortening of microtubules, a process termed dynamic instability, which has been observed both in vitro (*3*) and in vivo (*4*). Dynamic instability is thought to contribute to spindle morphogenesis and the reorganization of microtubule arrays during the cell cycle (*5*).

The tubulin-GTP cap model (*2, 3*) predicts that the GTPase activity of β-tubulin would be important in determining cap size and microtubule dynamics. To investigate the relation between guanosine triphosphatase (GTPase) activity and microtubule dynamics, we combined site-directed mutagenesis with a procedure for purifying assembly-competent tubulin from the yeast *Saccharomyces cerevisiae* (*6, 7*). We report on four mutations directed to the highly conserved region of β-tubulin, Lys^{103}-Gly-His-Tyr-Thr-Glu-Gly^{109} Sequence comparisons (*8*) suggest that this region may be functionally equivalent to the Gly-X-X-X-X-Gly-Lys motif of GTPase superfamily members, which participates in phosphate binding and hydrolysis. We substituted the conserved Lys^{103} with Met, a change that removed the charged amino group but retained the similar overall size and shape of the side group; substitution of Lys with Met in the $p21^{ras}$ Gly-X-X-X-X-Gly-Lys motif reduced that protein's GTPase activity (*9*). We also substituted β-tubulin Thr^{107} with Gly, Lys, or Trp because this amino acid modulates the GTPase activity of other superfamily members (*10*).

Because three of the mutations (Gly^{107}, Lys^{107}, and Trp^{107}) were lethal in haploid cells, we purified tubulin from heterozygous diploid strains (Table 1). In these strains, one β-tubulin gene was full-length (*TUB2* wild type or *TUB2*-derived mutant) and the other (*tub2-590*) was missing the last 12 codons (*11*). The *tub2-590* background allowed immunological detection of full-length β-tubulin with a rabbit polyclonal antibody to the COOH-terminal 12 amino acids of β-tubulin. The tubulin preparations were therefore composed of dimers with full-length (wild type or mutant, as appropriate) and truncated β subunits, in equal amounts (*12*). Purification of tubulin dimers containing only full-length β subunits could be accomplished chromatographically (*13*); however, the yields were too small to make the method routinely useful. The protein derived from each of the heterozygotes assembled into bona fide microtubules, and immunogold staining with the COOH terminal–specific antibody showed that both mutant and wild-type tubulins incorpo-

Department of Biological Sciences, University of California, Santa Barbara, CA 93106, USA.

*To whom correspondence should be addressed.

rated into the microtubules (Fig. 1A).

The steady-state rate of GTP hydrolysis of control microtubules (from a *TUB2/tub2-590* heterozygote) was 2,400 ± 1,200 P_i min^{-1} microtubule^{-1} (Table 1 and Fig. 1B), whereas the rates from the *tub2-T107G,K,W/tub2-590* microtubules were 4 to 10 times higher: 10,100 ± 2,400, 18,700 ± 6,100, and 23,500 ± 6,200 P_i min^{-1} microtubule^{-1}, respectively. In contrast, the rate for the *tub2-K103M/tub2-590* microtubules (3,100 ± 2,700 P_i min^{-1} microtubule^{-1}) was similar to that of control microtubules. The different hydrolysis rates of the mutated tubulin samples were not due to differential interactions of the mutated β-tubulins with the truncated *tub2-590* β-tubulin, because tubulin isolated from a *tub2-T107K/TUB2* strain also increased the microtubule hydrolysis rate as compared with tubulin from *TUB2/TUB2* wild-type microtubules (*14*).

According to the tubulin-GTP cap model (*2, 3*), an increased rate of GTP hydrolysis should reduce the average cap size at the microtubule end and so increase the probability that the cap will be lost. Loss of the cap would destabilize the microtubules, leading to an increase both in the steady-state critical concentration of tubulin and in microtubule dynamic instability. Conversely, no increase in either the critical concentration or microtubule dynamic instability would be expected for the *tub2-K103M/tub2-590* microtubules. Consistent with these predictions, the steady-state critical concentrations of microtubules with enhanced rates of GTP hydrolysis were 2 to 4 times greater than that of control microtubules and 7 to 12 times greater than that of the *tub2-K103M/tub2-590* microtubules (Table 1).

The three mutations with enhanced rates of GTP hydrolysis also increased microtubule dynamic instability, as measured by the time-dependent redistribution of microtubule lengths at polymer mass steady state, with the mean lengths increasing by 140 to 180% after the attainment of steady state (Fig. 2). There was no detectable length redistribution with control

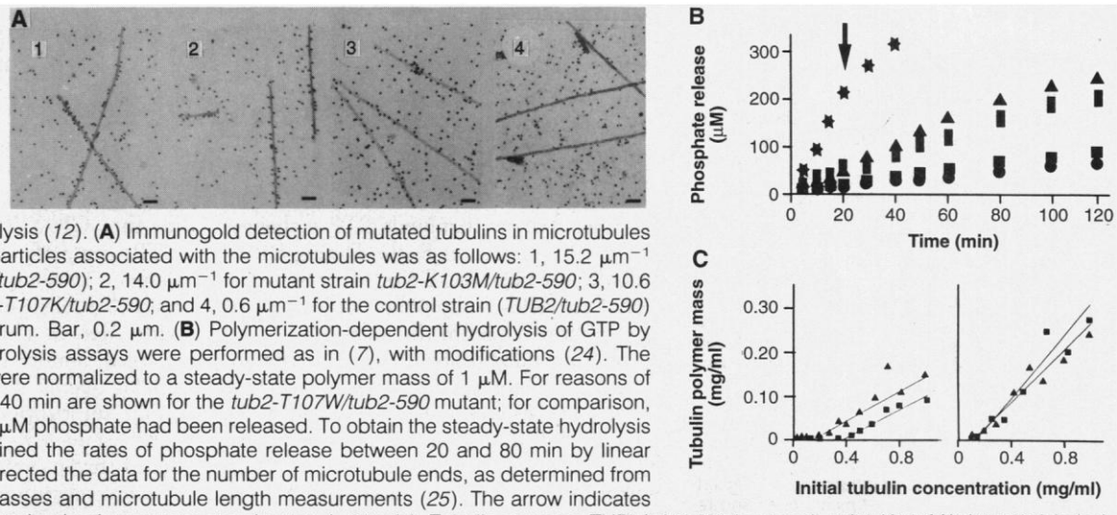

Fig. 1. In vitro polymerization properties of mutated and wild-type tubulins. The tubulin samples consisted of equal quantities of truncated (*tub2-590*–derived) and full-length (*TUB2*-derived) β-tubulins, as shown by quantitative protein blot analysis (*12*). (**A**) Immunogold detection of mutated tubulins in microtubules (*23*). The number of gold particles associated with the microtubules was as follows: 1, 15.2 μm^{-1} for the control strain (*TUB2/tub2-590*); 2, 14.0 μm^{-1} for mutant strain *tub2-K103M/tub2-590*; 3, 10.6 μm^{-1} for mutant strain *tub2-T107K/tub2-590*; and 4, 0.6 μm^{-1} for the control strain (*TUB2/tub2-590*) stained with preimmune serum. Bar, 0.2 μm. (**B**) Polymerization-dependent hydrolysis of GTP by mutated tubulins. GTP hydrolysis assays were performed as in (*7*), with modifications (*24*). The phosphate evolution data were normalized to a steady-state polymer mass of 1 μM. For reasons of scale, data for only the first 40 min are shown for the *tub2-T107W/tub2-590* mutant; for comparison, however, after 120 min 465 μM phosphate had been released. To obtain the steady-state hydrolysis rates (Table 1), we determined the rates of phosphate release between 20 and 80 min by linear regression analysis and corrected the data for the number of microtubule ends, as determined from the steady-state polymer masses and microtubule length measurements (*25*). The arrow indicates the time at which samples attained polymer mass steady state (~20 min). Tubulin sources: *TUB2/tub2-590* (squares), *tub2-K103M/tub2-590* (circles), *tub2-T107G/tub2-590* (rectangles), *tub2-T107K/tub2-590* (triangles), and *tub2-T107W/tub2-590* (stars). (**C**) The critical concentration for assembly of full-length wild-type and T107K β-tubulins in the presence of GTP (left) or GMPPCP (right). Because the *tub2-T107K* mutation was lethal in haploid cells, we purified (*13*) tubulin dimers containing full-length β-tubulin (*tub2-T107K* or *TUB2*) from dimers carrying the *tub2-590* truncated form. The critical concentrations were determined from the ordinate intercepts by linear regression analysis. For wild-type tubulin, with GTP and GMPPCP, the critical concentrations were 140 ± 4 μg ml^{-1} and 110 ± 23 μg ml^{-1}, respectively. The corresponding values for *tub2-T107K* mutated tubulin were 380 ± 5 μg ml^{-1} and 140 ± 34 μg ml^{-1}. Full-length wild-type tubulin (triangles), full-length *T107K* mutated tubulin (squares).

Table 1. In vitro properties of mutated yeast tubulins.

Genotype*	Steady-state GTP hydrolysis rate (P_i min^{-1} microtubule^{-1})†	GTP hydrolysis rate of unassembled tubulin (P_i min^{-1})†	Tubulin critical concentration (μg/ml)‡	GTP binding constant (nM)§	GTP binding stoichiometry (moles of GTP per mole of tubulin dimer)§
TUB2/tub2-590	2,400 ± 1,200	0.22 ± 0.03	120 ± 20	58 ± 7	1.04 ± 0.14
tub2-K103M/tub2-590	3,100 ± 2,700	0.05 ± 0.04	40 ± 30	59 ± 15	0.80 ± 0.12
tub2-T107G/tub2-590	10,100 ± 2,400	0.19 ± 0.10	500 ± 70	21 ± 2	1.00 ± 0.17
tub2-T107K/tub2-590	18,700 ± 6,100	0.15 ± 0.12	300 ± 70	16 ± 1	1.04 ± 0.15
tub2-T107W/tub2-590	23,500 ± 6,200	0.16 ± 0.07	500 ± 90	100 ± 31	1.13 ± 0.18

*All yeast strains were derived from the diploid ADY101 (*7*), which is homozygous for *tub2-590*. The mutations were directed to *TUB2* with mutagenic oligonucleotides (*20*) and were introduced into ADY101 by homologous transplacement to yield the heterozygous mutants. The presence of the mutations was confirmed by polymerase chain reaction sequencing of genomic DNA. †The assembly-dependent steady-state hydrolysis rates are corrected for background GTP hydrolysis by unassembled dimers. The background rates were determined by sedimentation of steady-state microtubules and measurement of hydrolysis rates in the supernatants. These supernatant values were then subtracted from the values for microtubule-containing samples. The values in the table are the means of three experiments ± 1 SEM. The nonassembly-dependent rates of GTP hydrolysis were determined at a tubulin concentration of 50 μg ml^{-1} and represent the intrinsic GTPase activities of unassembled dimers. ‡Tubulin critical concentrations were determined as in Fig. 1C. The values are the means of six to nine determinations ± 1 SEM. §GTP equilibrium binding affinities and stoichiometries were determined as in (*21*), modified for tubulin (*22*). Each value (± 1 SEM) was determined for at least five GTP concentrations (3 to 1000 nM).

microtubules [consistent with (7)] or with *tub2-K103M/tub2-590* microtubules. These results demonstrate that microtubule dynamics can be modulated by the assembly-dependent rate of GTP hydrolysis and support the idea that microtubule dynamics could be controlled by regulating the size of a tubulin-GTP (or GDP + P_i) cap.

The effects of the mutations are unlikely to be due to gross structural defects because (i) all mutated tubulins bound GTP with high affinities and with stoichiometries comparable to that of the control protein (Table 1); (ii) all mutated tubulins assembled into bona fide microtubules (Fig. 1A); (iii) wild-type and mutated tubulins displayed similar kinetics and patterns of proteolytic digestion with proteinase K at 40°C (14); and (iv) the steady-state critical concentrations for assembly of the wild-type and mutated tubulins were similar with the nonhydrolyzable GTP analog, GMPPCP, but were substantially different with GTP (Fig. 1C). A gross structural change would be expected to affect both GTP- and GMPPCP-induced assembly, whereas a specific effect on the mechanism of GTP hydrolysis should preferentially affect assembly with GTP.

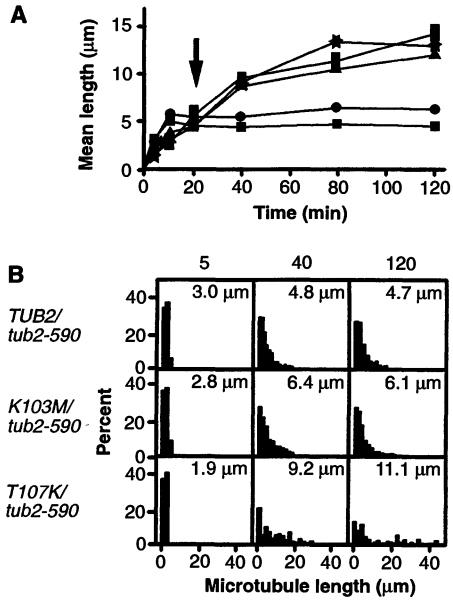

Fig. 2. The effects of β-tubulin mutations on the time-dependent redistribution of microtubule lengths at polymer mass steady state. (**A**) The mean lengths of the microtubule samples plotted as a function of time after assembly initiation. For each time point the lengths of 150 to 500 microtubules were measured. The arrow indicates the time at which polymer mass steady state was attained. Tubulin sources: *TUB2/tub2-590* (squares), *tub2-K103M/tub2-590* (circles), *tub2-T107G/tub2-590* (rectangles), *tub2-T107K/tub2-590* (triangles), and *tub2-T107W/tub2-590* (stars). (**B**) Representative microtubule length distributions at 5, 40, and 120 min after initiation of assembly. The mean lengths of the microtubule distributions are given in each box. The length distribution of the *tub2-T107K/tub2-590* mutant sample diverged substantially from the control and *tub2-K103M/tub2-590* mutant samples after attainment of steady state (at ~20 min), despite the similarity of the length distributions at the early time point (5 min). The results for tubulins isolated from the *tub2-T107G/tub2-590* and *tub2-T107W/tub2-590* mutants were similar to those for the *tub2-T107K/tub2-590* mutant.

Our data do not exclude the possibility that the mutations affect a site on β-tubulin that is remote from the GTP-binding pocket and yet affects microtubule dynamics and the rate of P_i formation. However, the effects of the mutations clearly show that the Lys^{103}-Gly-His-Tyr-Thr-Glu-Gly^{109} region of β-tubulin is important for the polymerization-dependent hydrolysis of GTP. Mutations in the Gly-X-X-X-X-Gly-Lys consensus motif of GTPase superfamily members also affect GTP hydrolysis (10); our results thus suggest that the Lys^{103}-Gly-X-X-X-X-Gly^{109} motif may be functionally equivalent to Gly-X-X-X-X-Gly-Lys, even though the sequence is reversed in β-tubulin. This situation may be comparable to that of the zinc metalloendopeptidases, where a conserved motif (His-Glu-X-X-His) has been found in both orientations at the active site (15). Other GTPases also display variant arrangements of the GTPase superfamily consensus motifs (16, 17).

The correlation between GTP hydrolysis rates and microtubule dynamics suggests that the β-tubulin GTPase activity could be regulated during mitosis to control microtubule depolymerization and chromosome movement. Increasing the tubulin GTPase activity at anaphase could lead to microtubule depolymerization which, in vitro experiments suggest (18), contributes to chromosome movement toward the spindle poles; similarly, chromosome congression to the metaphase plate could be facilitated if a higher rate of tubulin-GTP hydrolysis were maintained at kinetochores proximal to the plate. Opposing kinetochores of a single chromosome differ immunologically during chromosome movement toward the metaphase plate (19), suggesting that cellular mechanisms could exist for differentiating biochemical activities at opposing kinetochores.

REFERENCES AND NOTES

1. P. Dustin, *Microtubules* (Springer-Verlag, Berlin, ed. 2, 1987).
2. M. Carlier and D. Pantaloni, *Biochemistry* **20**, 1918 (1981).
3. T. Mitchison and M. Kirschner, *Nature* **312**, 232 (1984).
4. C. L. Rieder and S. P. Alexander, *J. Cell Biol.* **110**, 81 (1990).
5. M. Kirschner and T. Mitchison, *Cell* **45**, 329 (1986).
6. G. Barnes *et al.*, *Mol. Biol. Cell* **1**, 1 (1992).
7. A. Davis, C. R. Sage, L. Wilson, K. W. Farrell, *Biochemistry* **32**, 8823 (1993).
8. H. Sternlicht, M. B. Yaffe, G. W. Farr, *FEBS Lett.* **214**, 226 (1987).
9. I. S. Sigal *et al.*, *Proc. Natl. Acad. Sci. U.S.A.* **83**, 952 (1986).
10. A. Valencia, P. Chardin, A. Wittinghofer, C. Sander, *Biochemistry* **30**, 4637 (1991).
11. W. Katz and F. Solomon, *Mol. Cell. Biol.* **8**, 2730 (1988).
12. C. R. Sage and K. W. Farrell, unpublished data.
13. To separate dimers composed of the full-length and truncated β-tubulin forms, we fractionated tubulin from control (*TUB2/tub2-590*) or mutant (*tub2-T107K/tub2-590*) heterozygous strains by fast protein liquid chromatography (FPLC) with a Mono-Q column (Pharmacia) in 0.1 M Pipes (pH 6.9), 1.0 mM EGTA, 0.1 mM GDP over a 0.0 to 1.0 M NaCl gradient. Dimers containing full-length β subunits eluted at 0.22 to 0.26 M NaCl, and the truncated (*tub2-590*-derived) forms eluted at 0.26 to 0.29 M NaCl. To stabilize the fractions after elution, we immediately added glycerol (to 10% v/v) and $MgCl_2$ (to 1 mM). The tubulin samples were simultaneously desalted and concentrated in 0.1 M Pipes (pH 6.9), 1.0 mM EGTA, 1 mM $MgCl_2$ (PEM), 0.1 mM GDP with a Centricon 30 ultrafiltration cell (Amicon, Lexington, MA). Analysis of the β-tubulins by SDS–polyacrylamide gel electrophoresis and silver staining revealed that they were ≥95% full-length β-tubulins. Polymerization was induced in tubulin samples (25 to 1000 μg ml^{-1}) by the addition of 1 mM GTP or 10 mM GMPPCP and incubation at 30°C. The microtubules were assembled for 60 min and then sedimented (100,000*g*, 20 min at 30°C). Microtubule pellets were resuspended in 30 μl of ice-cold PEM, and critical concentrations for assembly were determined by Bradford protein assays.
14. A. Davis and K. W. Farrell, unpublished data.
15. A. B. Becker and R. A. Roth, *Proc. Natl. Acad. Sci. U.S.A.* **89**, 3835 (1992).
16. D. RayChaudhuri and J. T. Park, *Nature* **359**, 251 (1992).
17. B. Guy *et al.*, *ibid.* **330**, 266 (1987).
18. M. Coue, V. A. Lombrillo, J. R. McIntosh, *J. Cell Biol.* **112**, 1165 (1991).
19. G. J. Gorbsky and W. Ricketts, *ibid.* **122**, 1311 (1993).
20. T. A. Kunkel, J. D. Roberts, R. A. Zakour, *Methods Enzymol.* **154**, 367 (1987).
21. J. P. Hummel and W. J. Dryer, *Biochim. Biophys. Acta* **63**, 530 (1962).
22. A. Levi, M. Cimino, D. Mercanti, P. Calissano, *ibid.* **365**, 450 (1974).
23. For immunogold staining, the microtubules were fixed in PEM plus 30% (v/v) glycerol and 1% (v/v) glutaraldehyde and placed onto 100-mesh electron microscopy grids coated with collodion (Pelco Inc., Tustin, CA). The grids were blocked with cytochrome c (1.0 mg/ml) for 5 min, washed twice with distilled H_2O, and then incubated for 1.5 hours with an antibody specific for the COOH-terminal 12 amino acids of β-tubulin [1:300 dilution in 50 mM sodium phosphate buffer (pH 7.0), 50 mM NaCl]. The grids were washed twice with distilled H_2O, incubated for 1.5 hours with a 1:20 dilution of Protein A conjugated to 20-nm gold particles (Sigma), washed twice with distilled H_2O, and negatively stained with 1.5 M uranyl acetate. The number of gold particles per micrometer was determined from the electron micrographs over at least 100 μm of microtubule length. Background values were obtained from equal lengths of straight lines drawn at random on the photomicrographs and were subtracted from the microtubule-associated counts.
24. The modifications were as follows: (i) the FPLC-purified tubulin was used directly without a polymerization cycle because differences in the critical concentrations lead to selective enrichment or depletion of the mutated tubulins; and (ii) 500 μM GTP was used in all experiments with [γ-^{32}P]GTP at a specific activity of 40 to 50 Ci mol^{-1}.

25. K. W. Farrell, M. A. Jordan, H. P. Miller, L. Wilson, *J. Cell Biol.* **104**, 1035 (1987).
26. We thank R. Burns, M. A. Jordan, K. Middleton, B. Goode, and L. Wilson for critical reading of the manuscript and K. Sullivan for synthesizing the mutagenic oligonucleotides. Supported by NIH grant GM 41751 (to K.W.F.) and Department of Defense fellowship DAAL03-90-G0155 (to C.R.S.).

8 December 1993; accepted 17 March 1994

A Panoramic Code for Sound Location by Cortical Neurons

John C. Middlebrooks,* Ann E. Clock, Li Xu, David M. Green

By conventional spike count measures, auditory neurons in the cat's anterior ectosylvian sulcus cortical area are broadly tuned for the location of a sound source. Nevertheless, an artificial neural network was trained to classify the temporal spike patterns of single neurons according to sound location. The spike patterns of 73 percent of single neurons coded sound location with more than twice the chance level of accuracy, and spike patterns consistently carried more information than spike counts alone. In contrast to neurons that are sharply tuned for location, these neurons appear to encode sound locations throughout 360° of azimuth.

It often is assumed that dimensions of perception are represented in the brain by orderly maps containing sharply tuned neurons, and such maps are well known in the visual and somatosensory cortices. Maps of auditory space have been demonstrated at the level of the midbrain (*1*), but physiological studies of the auditory cortex have failed to demonstrate any evidence of a space map containing sharply tuned neurons. This has been puzzling, given that auditory cortex lesions in human patients and in experimental animals result in prominent deficits in sound localization behavior. In the inferior temporal and striate visual cortices, information-theoretic analysis has demonstrated that the spike patterns of neurons, including both spike count and spike timing, can carry nearly twice the stimulus-related information of spike counts alone (*2*). We studied spatial coding by auditory neurons in the cat's anterior ectosylvian sulcus cortical area (area AES). We used an artificial neural network to classify the spike patterns of single neurons according to sound source location. We found that single neurons can code for sound locations throughout 360° of azimuth.

Data were obtained from 67 single units on the posterior bank of the anterior ectosylvian sulcus of eight chloralose-anesthetized cats (*3*). Noise bursts, 1 to 300 ms in duration, were presented in an anechoic room from 18 loudspeakers spaced in 20° steps of azimuth around the horizontal plane. Stimulus locations were varied pseudorandomly to acquire 40 responses to stimuli at each of 18 sound source locations (for a total of 720 responses). Units responded with latencies greater than 10 ms, and their responses typically were restricted to the first 50 ms after stimulus onset; thus, nearly all the driven spikes fell within a time interval of 40 ms (*4*). To train the artificial neural network, we used the responses of single units on odd-numbered trials (20 trials per stimulus location). To test the network performance, we used the even-numbered trials from the same unit. This is a form of cross validation, in which training and testing utilized independent data sets.

The spike pattern elicited by a noise burst usually contained only a small number of spikes. The average spike counts at optimal loudspeaker locations were around three spikes per trial, yet even at such optimal locations, many stimulus presentations elicited no spikes at all. For that reason, we averaged the responses of a single neuron across multiple presentations of a given stimulus to estimate a spike density function. One way of computing this density function would have been to form, for each of the 18 stimulus locations, a single average of all 20 spike patterns in the training set and a single average of all 20 patterns from the test set. Under that condition, however, the network would have overtrained to idiosyncrasies in the set of 18 average training patterns. Moreover, the single set of test patterns would have provided only one pattern per stimulus location with which to evaluate network performance.

We adopted a different approach that utilized a "bootstrapping" procedure (*5*). We generated each bootstrapped training or test pattern by averaging across M patterns from the original data set of 20 training or test patterns, drawn randomly with replacement. Thus, a given bootstrapped pattern might incorporate zero, one, or more copies of any particular spike pattern. Repeating this process, we generated N_{train} bootstrapped training patterns from the training set and N_{test} bootstrapped test patterns from the test set. Network performance improved with increasing N_{train}, nearing an asymptote for values of N_{train} between 10 and 20, so we used a value of $N_{train} = 20$. We used $N_{test} = 100$ so that we could assess performance in terms of percent correct. In preliminary studies, we tested values of M (the number of spike patterns included in each bootstrap) between 1 and 32 and found that network performance improved monotonically with increases in the size of M; in the results presented here, we used M = 20. At each of the 18 stimulus locations, we generated a set of 20 bootstrapped training patterns and 100 bootstrapped test patterns.

The artificial neural network was a one-layer linear perceptron with 40 inputs, each corresponding to the estimated probability of a spike occurring in a 1-ms poststimulus time bin. Two output units formed a weighted sum of the 40 inputs. We used the Widrow-Hoff learning rule (*6*) to adjust the weights so that the output units produced the sine and cosine of the stimulus azimuth (*7*); the sine and cosine are proportional to the distance of the stimulus from the midsagittal plane and the interaural plane, respectively. For convenience in presenting network output, we computed the arctangent of the two outputs, which gave a continuously varying output in degrees of azimuth. We favored this simple network over more complex multilayer nonlinear nets because we found that it performed as well as more complicated nets and was less prone to overtraining.

By traditional measures of tuning based on spike counts, all of the units showed broad spatial tuning. For example, all but three of the units responded across at least 180° of azimuth with spike counts that were within 50% of their maxima, and the responses of 42% of the units never fell below 50% of their maxima, regardless of stimulus location. Despite this broad tuning of spike counts, the temporal spike patterns of most neurons varied systematically with sound location. Examples of the spike patterns elicited from one unit are shown in a raster plot in Fig. 1. Patterns varied both in spike count and spike timing. For this unit, the main feature of spike timing that varied with location was the overall latency of the burst, but the intertrial variability in the timing of spikes within patterns frustrated any effort to identify patterns simply on the basis of first-spike latency. The performance of the network, which used the timing of spikes throughout each burst to classify

J. C. Middlebrooks, A. E. Clock, L. Xu, Departments of Neuroscience and Otolaryngology, University of Florida Brain Institute, Gainesville, FL 32610–0244, USA. D. M. Green, Department of Psychology, Psychoacoustics Laboratory, University of Florida, Gainesville, FL 32611, USA.

*To whom correspondence should be addressed.